# Self-potential signals associated with pumping tests experiments

E. Rizzo,[1] B. Suski, and A. Revil

Département d'Hydrogéophysique et Milieux Poreux, Centre National de la Recherche Scientifique, Centre Européen de Recherche et d'Enseignement de Géosciences de l'Environnement, Université d'Aix-Marseille III, Aix-en-Provence, France

S. Straface and S. Troisi

Soil Conservation Department, University of Calabria, Cosenza, Italy

Received 26 February 2004; revised 30 June 2004; accepted 12 July 2004; published 7 October 2004.

[1] The flow of groundwater during a pumping test experiment is responsible for a measurable electrical field at the ground surface owing to the electrokinetic coupling between the Darcy velocity and the electrical current density. This electrical field can be measured passively with a network of nonpolarizable electrodes connected to a digital multichannel multimeter with a high internal impedance (>10 Mohm). These so-called self-potential signals can be used to track the pattern of groundwater flow in the subsurface. A field test was performed using a set of 53 $Pb/PbCl_2$ electrodes plus an additional electrode used as a unique reference in the field and a set of five piezometers to monitor the position of the piezometric surface. Using appropriate Green's functions, the electrical response is analyzed in terms of piezometric head distribution. This new methodology, which we call "electrography," allows visualization of preferential fluid flow pathways and the distribution of heads during pumping test experiments. Using a conditioning technique, this method could allow inversion of the hydraulic conductivity distribution around a pumping well. *INDEX TERMS:* 0925 Exploration Geophysics: Magnetic and electrical methods; 1832 Hydrology: Groundwater transport; 5104 Physical Properties of Rocks: Fracture and flow; 5109 Physical Properties of Rocks: Magnetic and electrical properties; 5114 Physical Properties of Rocks: Permeability and porosity; *KEYWORDS:* self-potential, pumping test, transmissivity

**Citation:** Rizzo, E., B. Suski, A. Revil, S. Straface, and S. Troisi (2004), Self-potential signals associated with pumping tests experiments, *J. Geophys. Res.*, *109*, B10203, doi:10.1029/2004JB003049.

## 1. Introduction

[2] In hydrogeology, the information related to hydraulic transmissivity is usually obtained from pumping test experiments [*Domenico and Schwartz*, 1997] and downhole measurements [*Rabaute et al.*, 2003]. However, all these methods are intrusive and the hydrological system is perturbed by the presence of the boreholes. One of the goals of geophysics is to image the interior of the Earth using nonintrusive techniques. Mainly in the last decade, hydrogeologists have started to use geophysical information in groundwater flow parameter estimation [e.g., *Cassiani and Medina*, 1997; *Cassiani et al.*, 1998; *Troisi et al.*, 2000, and references therein]. Because the flow of groundwater generates a detectable electrical field in the subsoil, hence at the ground surface of the Earth [e.g., *Sill*, 1983; *Fournier*, 1989; *Birch*, 1993, 1998; *Aubert and Yéné Atangana*, 1996; *Titov et al.*, 2000; *Perrier et al.*, 1998, 2002], it should be possible to invert this electrical field to obtain an information relative to the pattern of the groundwater flow. The basic idea for such a method, which *Revil et al.* [2003a] have called electrography, has haunted the literature for a long period of time. For example, *Poldini* [1938] showed qualitatively the relationship between self-potential signals and the flow of the groundwater. Nowadays, the underlying physics describing the coupling between the flow of water through a porous continuum and the generation of an electrical field is well understood at the scale of the representative elementary volume of the porous continuum and described by the electrokinetic theory [e.g., *Bernabé*, 1998; *Lorne et al.*, 1999]. At the scale of the geological system, the forward electromagnetic problem can be stated as a classical potential field problem [e.g., *Fitterman*, 1978, 1979], and various algorithms have been developed in the last years to determine the source distribution responsible for the electrical potential anomalies recorded at the ground surface. Of course, like any potential field problem, the inverse problem is ill-posed and suffers from nonuniqueness of the solution. To remove this nonuniqueness, the maximum of information regarding the physical process at play and the combination of self-potential with other nonintrusive techniques or in situ sources of information in boreholes is of course welcome.

[3] Recently, research scientists have been interested in developing interpretation schemes that could be applied to the electrical field recorded during pumping tests [e.g., *Titov*

[1]Now at Institute of Methodologies for Environmental Analysis, Institute of Methodologies for Environmental Analysis, Consiglio Nazionale delle Ricerche, Potenza, Italy.


0148-0227/04/2004JB003049$09.00

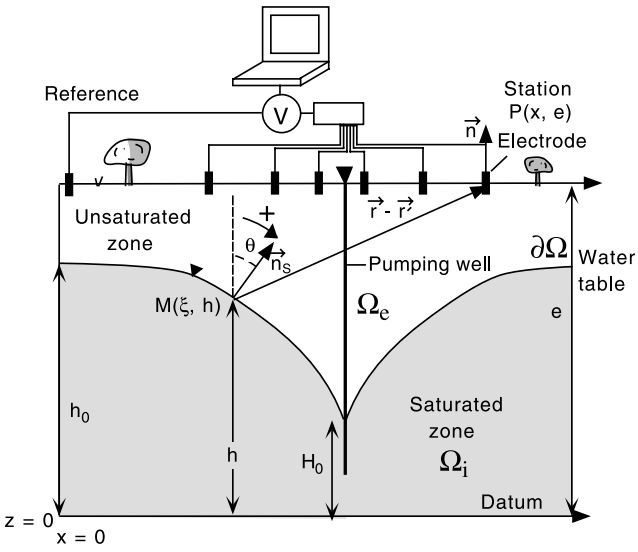


**Figure 1.** Monitoring of the electrical response associated with a depression cone of an unconfined aquifer. The reference electrode is taken as far as possible from the pumping well. Two electrokinetic contributions are associated with pumping. The former is associated with the shape of the water table, while the second is directly associated with the pumping. These two contributions are expected to generate positive self-potential anomalies at the ground surface. In addition to these electrokinetic contributions, the metallic casing of the borehole can be responsible for static negative self-potential anomalies associated with corrosion of the metallic casing (electro-redox component).

*et al.*, 2002]. For example, *Revil et al.* [2003a] and *Darnet et al.* [2003] analyzed the data by *Bogoslovsky and Ogilvy* [1973] in order to determine the piezometric level distribution and the hydraulic conductivity of the subsoil. However, there is a notorious lack of information regarding the field data described by *Bogoslovsky and Ogilvy* [1973] to test the models. The same is true of the equally interesting contour data shown by *Semenov* [1980, Chapter XI]. A number of other investigators have addressed the calculation of the self-potential response of a pumping well [e.g., *Friborg*, 1996; *Wilt and Butler*, 1990; *Sheffer*, 2002; *Sheffer and Howie*, 2001, 2003]. However, most of these studies used very simple assumptions (a point flow source or sink in a uniform half-space) and did not investigated the relaxation phase following the shutdown of the pump.

[4] Clearly, additional field measurements are crucially needed to push these ideas one step further. The basic idea underlying these investigations is as follows. Pumping tests, with a set of monitoring piezometers, represent the most common method to determine the flow and transport properties of rocks and sediments in the shallow subsurface of the Earth [e.g., *Domenico and Schwartz*, 1997]. However, their main drawback is the high cost of piezometers and the fact that the observed response is perturbed by the presence of the boreholes themselves as, indeed, a borehole represents a highly permeable vertical flow pathway that perturbs the hydraulic response (even for cased wells). In addition, the scarcity of the data calls for some additional information that could be added to the pure hydrogeological information to obtain a better representation of the hydraulic properties [e.g., *Cassiani and Christakos*, 1998]. Consequently, the reliability and interpretation of piezometric data often are problematic. On the other hand, self-potential measurements necessitate a set of nonpolarizable electrodes placed at the ground surface. There are two advantages in these measurements: (1) the self-potential method is nonintrusive and (2) the sensor, i.e., the electrode, is cheap. Therefore it is possible to use a large number of sensors at the ground surface, which is a very important advantage from the viewpoint of inverse theory and stochastic estimation techniques.

[5] In this paper, we present a new analytical solution to the coupled hydroelectric problem associated with a pumping test (section 2). New field data are presented from a test site located in Calabria (southern Italy) (section 3). The test was performed in July 2003 and includes both the monitoring of the piezometric response together with the electrical response. The results open exciting perspectives regarding our possibility to monitor groundwater flow using the self-potential method. The validation of the underlying physics has many other applications in the areas of potential electromagnetic precursors of earthquakes [e.g., *Corwin and Morrison*, 1977; *Fujinawa et al.*, 2002] and volcanic eruptions [e.g., *Revil et al.*, 2003b, 2004]. In both cases, fluid flow could be associated with (thermo) hydromechanical coupling and in turn is responsible for electromagnetic disturbances that can be recorded at the ground surface of the Earth. However, these topics remain rather controversial.

## 2. Theory

[6] In this section, we provide a model linking self-potential signals to groundwater flow in both the steady state pumping conditions and during the relaxation of transient recovery condition after the shutdown of the pump. These models will be used to interpret field data in section 3.

### 2.1. Constitutive and Continuity Equations

[7] In an isotropic porous material, the total electrical density $\mathbf{J}$ is the sum of a conductive current, described by the Ohm's law, and a net (or driving) source current density $\mathbf{J}_S$, which is associated with the pore fluid pressure field [e.g., *Sill*, 1983],

$$\mathbf{J} = -\sigma(\nabla\varphi - C\nabla p) \tag{1}$$

$$C \equiv -L/\sigma, \tag{2}$$

where $\varphi$ is the electrical potential (in V), $\sigma$ is the electrical conductivity (in S $m^{-1}$) (granular sediments [e.g., *Revil et al.*, 1998]), $C$ is the classical electrokinetic coupling coefficient (expressed in V $Pa^{-1}$), $L$ is an electrokinetic coupling term [e.g., *Fitterman*, 1978, 1979; *Revil et al.*, 2003a], and $\mathbf{J}_S = \sigma C\nabla p$ is the electrokinetic current density (in A $m^{-2}$), which acts as a source term for electromagnetic disturbances in the Maxwell equations. We note $\Omega_i$ and $\Omega_e$ the internal and external volumes of the source body in which fluid flow occurs, and $\partial\Omega$ the boundary between $\Omega_i$ and $\Omega_e$ (Figure 1). Using the constitutive equation (1) and

the continuity equation $\nabla \cdot \mathbf{J} = 0$ (conservation of charge in the quasi-static limit), we obtain

$$\nabla \cdot (\sigma \mathbf{E}) = \Im \tag{3}$$

$$\Im = -\nabla \cdot (C\sigma \nabla p) = \nabla L \cdot \nabla p + L\nabla^2 p, \tag{4}$$

where $\mathbf{E} = -\nabla\varphi$ represents the electrical field in the quasi-static limit of the Maxwell equations and $\Im$ (in A $m^{-3}$) represents the volumetric density of current source [e.g., *Furness*, 1992].

[8] In the zone of saturation, the driving force for groundwater flow is the hydraulic head $h$ related to the elevation head $z$ and to the pressure head, $\psi \equiv p/\rho_f g$, by $\psi = h - z$ [e.g., *Domenico and Schwartz*, 1997]. The electro-osmotic contribution to groundwater flow is orders of magnitude smaller than the pressure head contribution in most rocks in absence of external sources of electrical field [e.g., *Sill*, 1983]. Neglecting this contribution, the fluid flow is governed by the classical diffusion equation [e.g., *Domenico and Schwartz*, 1997, chapter 4]

$$\nabla^2 h - \frac{S_S}{K}\frac{\partial h}{\partial t} = \frac{Q}{K} \tag{5}$$

$$S_S = \rho_f g\left(\beta_p + \phi\beta_f\right), \tag{6}$$

where $K = k\rho_f g/\eta_f$ is the hydraulic conductivity (in m $s^{-1}$), $S_S$ is the specific storage (in $m^{-1}$), $\beta_p$ is the pore compressibility, and $\beta_f$ is the pore water compressibility [*Domenico and Schwartz*, 1997, Chapter 4]. Therefore the volumetric density of current source is simply

$$\Im = -\nabla \cdot \mathbf{J}_S \tag{7}$$

$$\Im = \rho_f g\left[\nabla L \cdot \nabla h + L\nabla^2 h\right]. \tag{8}$$

In sections 2.2 and 2.3 we investigate separately the situations for steady state pumping conditions and for the relaxation of the phreatic surface, respectively.

### 2.2. Pumping Test in Steady State Conditions

[9] In this case we consider our aquifer as unconfined. In steady state conditions for a pumping well, the first term of the volumetric current in equation (8) is zero as $L$ is constant through the water table. Indeed, in this situation the phreatic surface is a streamline and the gradient of the piezometric head is parallel to the piezometric surface. Using equation (8) and $\nabla L \cdot \nabla h = 0$, we obtain in steady state conditions $\Im = \rho_f g L \nabla^2 h$. Under the Dupuit's assumption for an homogeneous unconfined aquifer, the piezometric head $h(r)$ at distance $r$ from the pumping boreholes, for steady radial flow, is [e.g., *Verruijt*, 1970]

$$h(r) = \left(H_0^2 + \frac{Q}{\pi K}\ln(r/r_0)\right)^{1/2}, \tag{9}$$

where $Q$ is the volumetric pumping rate, $H_0$ is the hydraulic head in the pumping well, and $r_0$ is the radius of the pumping well. Using equation (9) and $\Im = \rho_f g L \nabla^2 h$ yields

$$\Im(r) = -\frac{\rho g L Q^2}{4\pi^2 K^2 r^2\left(H_0^2 + \frac{Q}{\pi K}\ln(r/r_0)\right)^{3/2}}. \tag{10}$$

In the geometry shown in Figure 1, the continuity equation becomes

$$\nabla \cdot (\sigma \mathrm{E}) = \begin{cases} \Im(r), & \mathbf{r} \in \Omega_i \\ 0, & \mathbf{r} \in \Omega_e. \end{cases} \tag{11}$$

We assume a constant conductivity distribution in the conductive half-space below the ground surface (Figure 1). The upper half-space above the ground surface is considered to be a good insulator and the boundary condition at the ground surface is $\mathbf{n} \cdot \nabla\varphi = 0$, i.e., the electrical field is everywhere tangential to the ground surface where it is measured. With these assumptions, equation (11) is written as

$$\nabla^2 \varphi = \begin{cases} -\Im(r)/\sigma_i, & \mathbf{r} \in \Omega_i \\ 0, & \mathbf{r} \in \Omega_e, \end{cases} \tag{12}$$

where we do not account for any surface of electrical conductivity discontinuity in the region $\Omega$ external to the source volume. According to equation (12), the electrical potential is harmonic outside the source volume. The Green's function of the Poisson equation is solution of,

$$\nabla^2 G(\mathbf{r}, \mathbf{r}') = \delta(\mathbf{r}'), \tag{13}$$

where $\delta(\mathbf{r}')$ represents the Dirac distribution at source point $\mathrm{M}(\mathbf{r}')$. The 3-D and 2-D Green's functions for an homogeneous half-space with no topography are

$$G(\mathbf{r}, \mathbf{r}') = -\frac{1}{2\pi}\frac{1}{|\mathbf{r} - \mathbf{r}'|} \tag{14}$$

$$G(\mathbf{r}, \mathbf{r}') = \frac{1}{2\pi}\ln(\mathbf{r} - \mathbf{r}')^2 \tag{15}$$

in three and two dimensions, respectively. Application of Green's theorem to the previous boundary value problem yields [e.g., *Sobolev*, 1989, p. 297]

$$\varphi(\mathbf{r}) = -\frac{1}{\sigma_i}\int_{\Omega_i} G(\mathbf{r}, \mathbf{r}')\Im(\mathbf{r}')dV, \tag{16}$$

and the necessary and sufficient condition for this problem to have a solution is

$$\int_{\Omega_i} \Im(\mathbf{r}')dV = \int_{\Omega_i} \nabla^2 h(\mathbf{r}')dV = 0, \tag{17}$$

obtained by the continuity equation for the mass of water in steady state conditions.

[10] The electrical potential can only be measured to a reference electrode (where $\varphi_0 = 0$ by definition). We assume that this reference electrode is outside the "electrical radius of influence" of the pumping well so the reference electrode can be considered to be at infinity. From now, we consider that the casing of the borehole has an infinite conductivity (metallic casing). Assuming the ground being homogeneous, the electrical potential depends only on the distance $r$ from the borehole. Integrating equation (16) yields

$$\varphi(\mathbf{r}) = -\frac{1}{2\pi}\int_{\Omega_i} \frac{\rho_f g L Q^2 r' dr' d\theta dz}{4\pi^2 K^2 \sigma_i r'^3 \left[H_0^2 + \frac{Q}{\pi K}\ln(r'/r_0)\right]^{3/2}}, \quad (18)$$

$$\varphi(\mathbf{r}) = \int_{R_b}^{r}\int_{Z-h(r')}^{Z} \frac{C' Q^2 dr' dz}{4\pi^2 K^2 r'^2 \left[H_0^2 + \frac{Q}{\pi K}\ln(r'/r_0)\right]^{3/2}}, \quad (19)$$

$$\varphi(\mathbf{r}) = \left(\frac{C' Q^2}{4\pi^2 K^2}\right)\int_{R_b}^{r} \frac{dr'}{r'^2\left[H_0^2 + \frac{Q}{\pi K}\ln(r'/r_0)\right]}, \quad (20)$$

where $R_b$ is the borehole radius and $C' \equiv (\partial\varphi/\partial h)_{\mathbf{J}=0} = -\rho_f g L/\sigma$ is the electrokinetic coupling coefficient associated with pressure head variations (in V m$^{-1}$). In the Dupuit approximation, the drawdown is relatively small. If we neglect the drawdown, the electrical potential response is given by the following first-order approximation:

$$\varphi(r) \approx -\frac{1}{r}\left(\frac{C' Q^2}{4\pi^2 K^2 H_0^2}\right). \quad (21)$$

This solution is similar to that obtained for a fully penetrating well (e.g., a line fluid sink or source). This provides a new analytical solution to determine the self-potential signals associated with pumping in a metallic cased well. Note that the electrical response diverges at $r = 0$ as we have assumed that the electrical conductivity of the casing of the borehole is infinite. Because the electrokinetic coupling coefficient $C'$ is generally negative, the resulting self-potential anomaly around the pumping well is expected to be positive according to equation (21). In addition this model predicts that the self-potential is inversely proportional to the inverse of the hydraulic conductivity square. Therefore the method is expected to be quite sensitive to the equivalent permeability of the aquifer if not to the permeability distribution.

### 2.3. Recovery Test

[11] We look now for the electrical response associated with the relaxation of the phreatic surface when the pump is shutdown. In this case, the measured electrical potential at the observation point P is [*Fournier*, 1989; *Birch*, 1993, 1998; *Revil et al.*, 2003a]

$$\varphi(\mathbf{r}) \approx \frac{C'}{2\pi}\int_{\partial\Omega} h(\mathbf{r}')\left(\frac{\mathbf{n}_S(\mathbf{r}')\cdot(\mathbf{r}-\mathbf{r}')}{|\mathbf{r}-\mathbf{r}'|^3}\right)dS, \quad (22)$$

where the electrokinetic coupling coefficient in the vadose zone can be neglected. According to equation (22), each element of the water table can be seen as a small dipole with strength proportional to the piezometric level. If the water table variation is relatively small and if the solid angle from which the water table (i.e., the source surface) is seen from the observation point P is approximately equal to $2\pi$ (in three dimensions), we obtain from equation (22) a first-order (and very simple) linear approximation on the form

$$\delta\varphi(\mathbf{r}) \approx C'(h(\mathbf{r}) - h_0), \quad (23)$$

where $h_0$ is the hydraulic head where the reference electrode is taken. After the shutdown of the pump and according to equation (23), the electrical potential is proportional to the piezometric level. In transient conditions, we consider our aquifer as confined. So the residual drawdown, at a fixed point, is given by [*Domenico and Schwartz*, 1997, chapter 6, p. 114]

$$\delta s \equiv h_0 - h = \frac{2.3Q}{4\pi T}\log\left(\frac{t}{t'}\right), \quad (24)$$

where $h_0$ is the initial hydraulic head, $T$ is the hydraulic transmissivity, $t'$ is the time since pumping stopped, $t = t' + \delta t$ is the time since pumping started, and $\delta t$ is the duration of the pumping test ($\delta t$ = 5854.7 min here). Therefore, under the validity of the assumptions underlying equations (23) and (24), the electrical potential is given by

$$\delta\varphi = -\frac{C' 2.3Q}{4\pi T}\log\left(\frac{t}{t'}\right) \quad (25)$$

and can be used, in principle, as a proxy for the direct measurements of the piezometric surface. This idea will be tested in section 3.4.

## 3. Field Experiment

[12] The test site is located near the town of Montalto Uffugo, in the region of Calabria in Southern Italy. The precise location of the field is given by *Troisi et al.* [2000] and will not be repeated here. The experiment consisted in a classical pumping test in which the piezometric response was recorded in a set of monitoring piezometers (see location in Figure 2). We also measured the electrical response at the ground surface with a monitoring network of 53 electrodes connected to a multimeter and a reference electrode (Figures 3 and 4).

### 3.1. Geological Setting and Description of the Experiment

[13] The geology of the test site can be divided in four geological formations (Figure 2). Heterogeneous gravels in a silty sand matrix (formation A) compose the first forma-

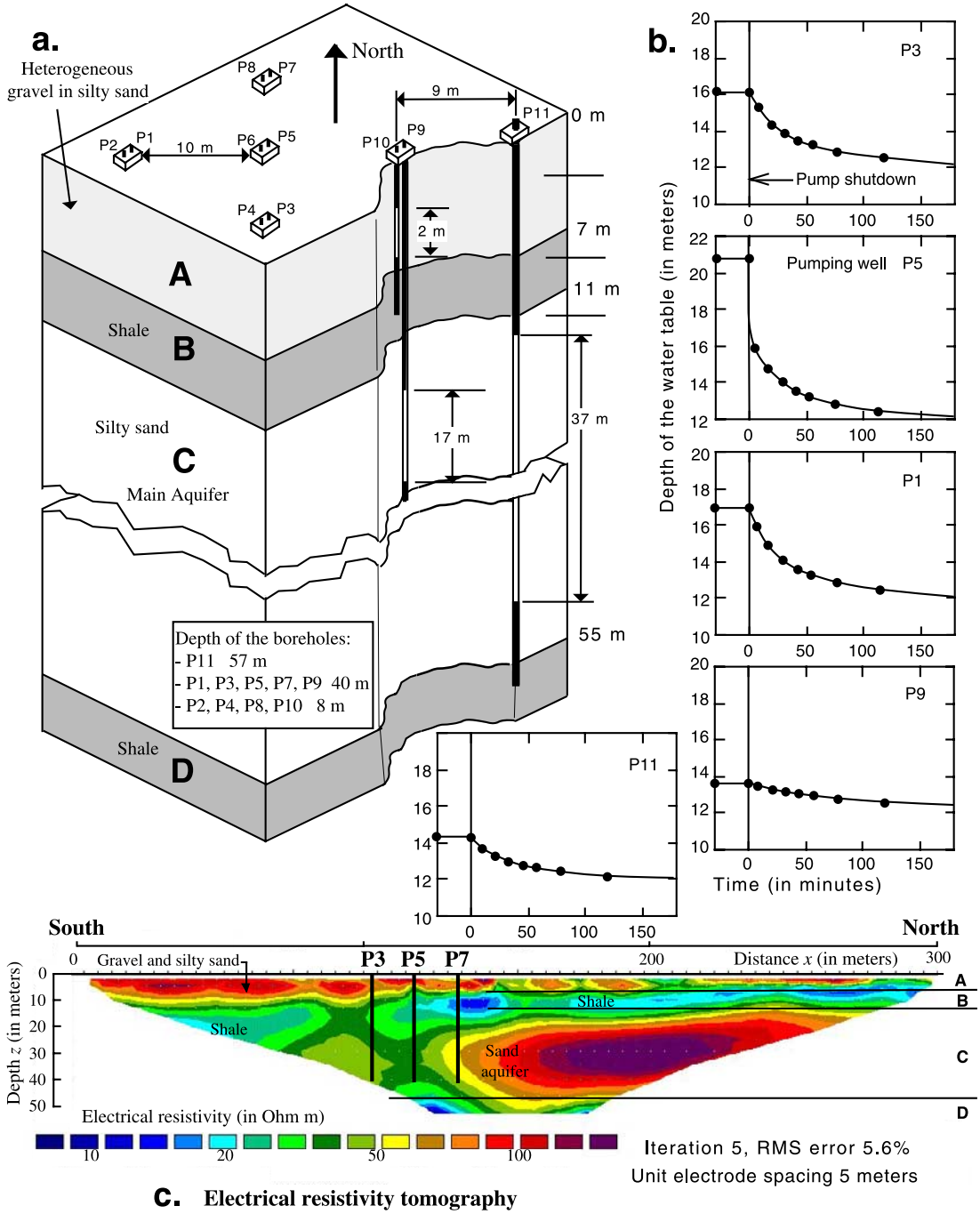


**Figure 2.** Sketch of the test site. (a) The test site comprising five monitoring units, each unit being composed of a 40 m deep well plus a 10 m deep piezometer. The central monitoring unit (P5 is the pumping well) is surrounding by four monitoring units created in June 1993. An additional borehole coded P11 was drilled in October 1997 to a depth of 57 m. Borehole P11 penetrates the shale unit underlying the confined aquifer. (b) Relaxation of the phreatic surface after the shutdown of the pump. (c) Electrical resistivity tomography distinctly showing the different geological formations. The shale appears with a low electrical resistivity due to the high interfacial (surface) conductivity associated with the high cation exchange capacity. The tomography also shows the heterogeneity of the main aquifer. In the main aquifer, the higher the resistivity, the lower the hydraulic conductivity.

tion. This formation extends from the ground surface to a depth of ~7 m. The second formation is a shale layer (formation B in Figure 2, from ~7 to ~11 m). The third formation bears the main aquifer investigated in this paper and is composed by a silty sand layer (layer C, from 11 to 55 m). The deepest formation is the shale substratum (formation D) (Figure 2). A shallow perched aquifer is sometimes present during part of the year in formation A. This was the case at the time of our experiment but the drawdown is below (not above) the shale layer.

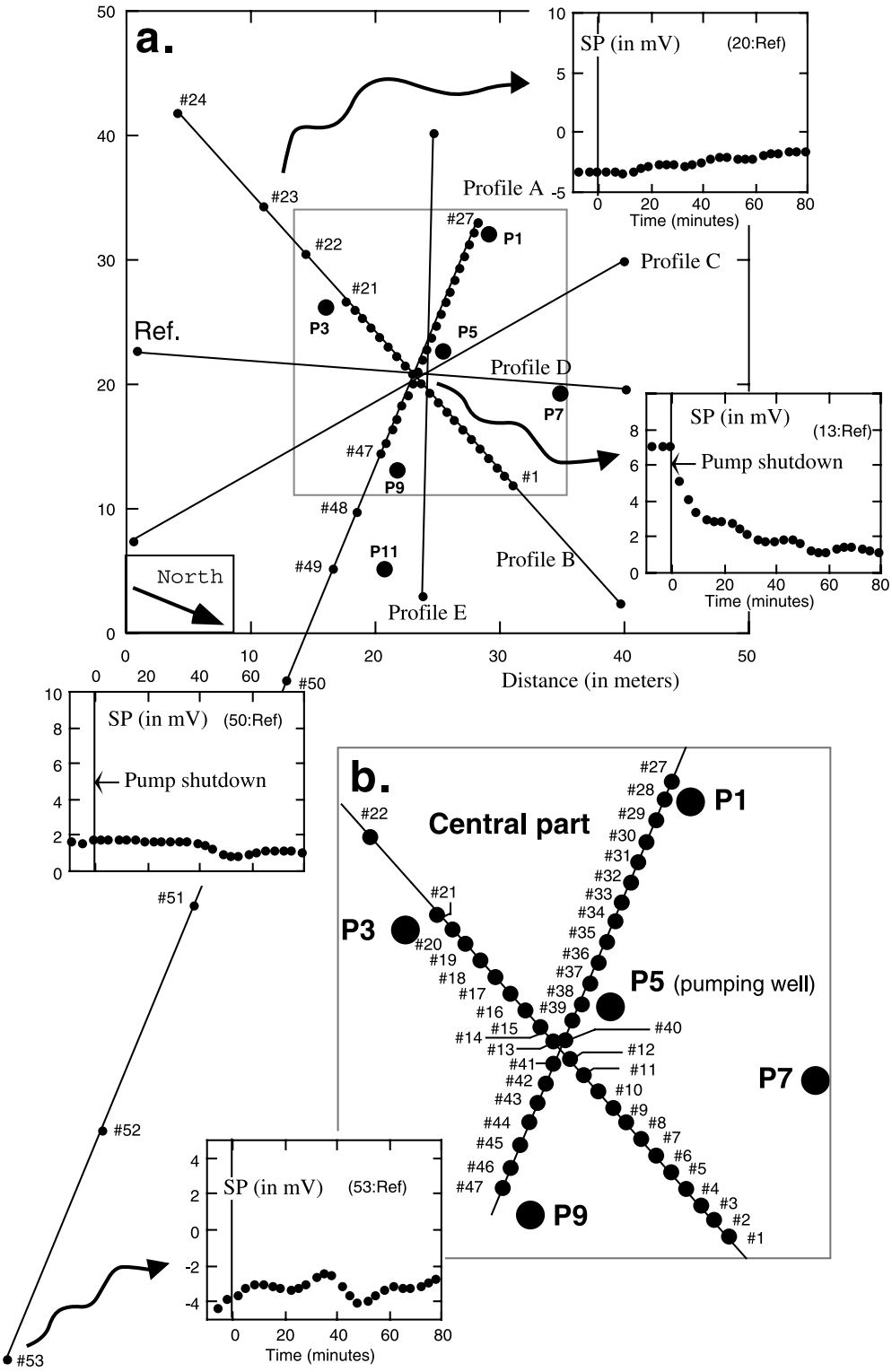


**Figure 3.** Position of the electrodes during the monitoring experiment (view from above). (a) Overall view of the acquisition network of electrodes. (b) Magnification of the electrode network in the vicinity of the pumping well. P5 is the pumping well, and P1, P3, P7, P9, and P11 are the monitoring piezometers. Some typical self-potential variations are also shown at different electrodes located at different distances from the pumping well ("Ref" is the reference electrode used during the measurements).

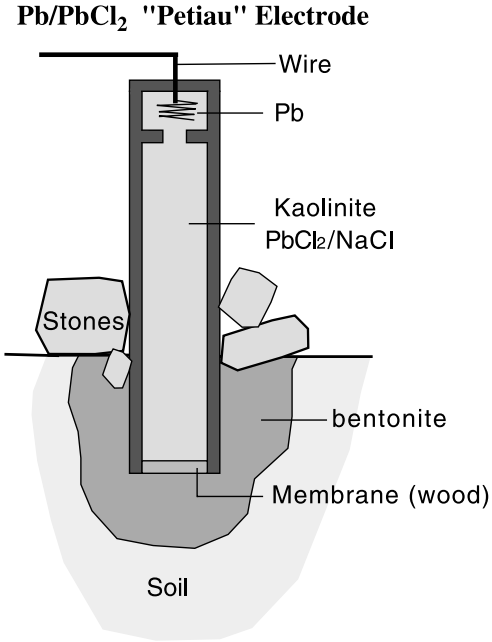


**Figure 4.** Self-potential monitoring station. Each station is composed of a $Pb/PbCl_2$ electrode placed in a small hole filled with a bentonite mud. The high electrical conductivity of bentonite and its very low hydraulic conductivity insure good electrical contact and constant moisture conditions during the experiment. Some stones are placed around the electrodes to decrease the dryness of the mud by direct contact with the sunlight.

[14] Ten boreholes (two boreholes per monitoring location) have been drilled at this test site. They are numbered P1 to P10 and they have all a metallic casing. The locations of the boreholes are shown in Figure 2. Each pair includes a borehole reaching a depth of 8 m (i.e., reaching the shallow perched groundwater) and a second borehole reaching a depth of 40 m and is therefore connected to the aquifer of interest. Moreover, there is an additional borehole coded P11 and located 19 m from the central well P5 and reaching the impervious bottom of the main aquifer (Figure 2). The diameter of the pumping well is 20 cm.

[15] The experiment was performed in July 2003. Prior the experiment, pressure sensors were placed in the monitoring piezometers (except in P5) to record the hydraulic head every 5 min during the pumping test experiment. The piezometric levels were also measured directly during the course of the experiment. The pumping experiment involved the main aquifer and was performed to obtain a steady state drawdown of several meters below formation B (i.e., above the upper shale layer). The pumping rate $Q$ was equal to 2.7 L $s^{-1}$ in P5, achieving the steady state conditions in $\sim$4 days. In steady state conditions, pressure sensors located into the boreholes provided directly the depth of the water table.

[16] The monitoring of the self-potential signals was carried out using 53 nonpolarizable $Pb/PbCl_2$ "Petiau" electrodes manufactured by SDEC in France (see *Perrier et al.* [1997] and *Petiau* [2000] for analysis of the stability of these electrodes). The electrodes were located along two profiles crossing each other in the vicinity of the pumping well (Figure 3). One electrode was used as a fixed reference station (Ref) in the field (Figure 3). To have uniform ground contact conditions for all electrodes, we dug small holes (around 10 cm deep), filled with a salty bentonite mud and covered with several small stones in order to keep the moisture conditions high during the whole monitoring experiment (the day of the experiment was very hot) (Figure 4). All electrodes were connected with a high internal impedance (>10 Gohm) multimeter (Keithley 2701) (Figure 1). The multimeter was interfaced to a notebook computer to observe the data acquisition in real time. The data were acquired automatically with a time step of 1 min. Recording of self-potential signals starts at 1017 LT. The pump was shut off at 1038 LT and the monitoring was performed during several hours.

[17] Note that if the electrodes do not experience the same temperature, a small potential drift can occur due to a thermoelectric effect. According to the supplier (SDEC), the temperature drift of the Petiau electrodes is 0.2 mV/°C. So a temperature difference of 5°C can be responsible for a self-potential drift of 1 mV, which is a substantial value when compared with the strength of the electrokinetic component associated with groundwater flow and described below (<10 mV). This explains why great care should be taken when placing the electrodes in the field especially regarding their exposure to sunlight. The electrode readings also can be affected by drying of the surrounding soil and by precipitations. Covering each of the electrodes with small, inverted styrofoam, weighted down by small stones, helps to reduce these effects (R. Corwin, personal communication, 2004).

### 3.2. Results

[18] Before the monitoring experiment, we performed a self-potential map while the pumping was operating in steady state conditions (profiles A to E, Figure 3). The results are shown in Figure 5a. We performed a similar map at the end of the experiment after the relaxation of the phreatic surface (Figure 5b). The two maps show two quite strong ($\sim$80 mV in magnitude) negative self-potential anomaly centered at wells P5 and P9 with smaller signals on the other wells except P11. The static self-potential map was roughly the same during steady state pumping conditions and at the end of the experiment. This excludes that the main contribution to this signal was due to groundwater flow and electrokinetic coupling. Because the standard deviation for the measurements in doing such a static self-potential map is high (5 mV in the present case), we can expect that the self-potential signals associated with groundwater flow to be much smaller than the amplitude of this signal.

[19] To understand the origin of these static self-potential anomalies, we must recall that self-potential anomalies are caused usually by two different charging mechanisms occurring in the subsurface of the Earth. A general theory of current source density has been obtained recently by *Revil and Leroy* [2004]. The first source is related to groundwater flow (electrokinetic contribution), while the second contribution is associated with oxido-reduction processes (electro-redox contribution). This second contribution is due to corrosion of the metallic casing of the boreholes, which can be helped by the presence of biofilms.

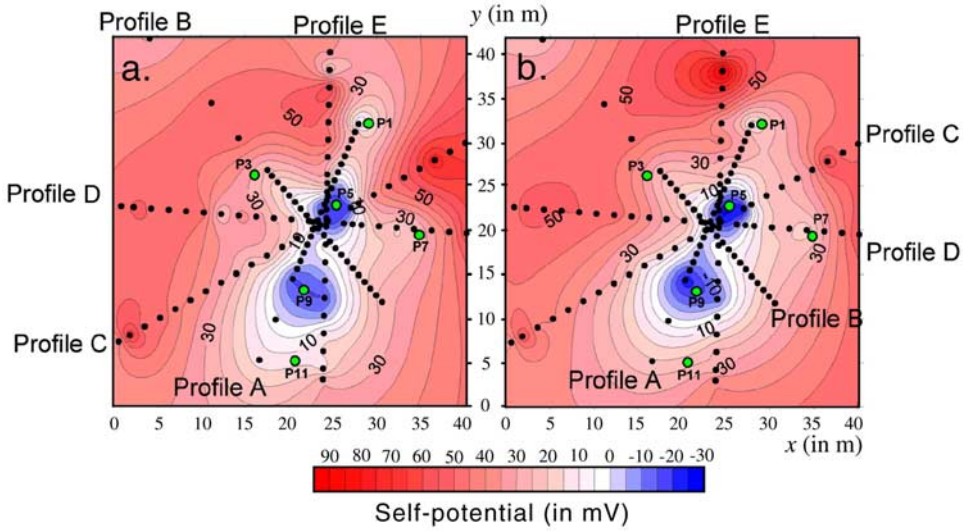


**Figure 5.** Self-potential maps (a) during the pumping test (steady state conditions) and (b) after the pump shutdown at the end of the relaxation of the phreatic surface. The small black circles indicate the position of the measurement points. For each location, a small hole was dug and filled with bentonite mud to improve the contact between the electrode and the ground. The main source of the signal is an electro-redox contribution, which is known to produce negative self-potential signals. The electrokinetic component is 1 order of magnitude smaller than this contribution. Note that all the boreholes drilled in 1993 exhibit some negative self-potential anomalies (with differing extent), while well P11, drilled later in 1997, does not seem to show any static self-potential anomalies (note that the reference for the maps is arbitrarily taken close to piezometer P1). Finally, the difference between the data sets of Figures 5a and 5b cannot be compared with those of Figure 11 as the standard deviation associated with self-potential mapping (~5–10 mV) is too high by comparison with the strength of the electrokinetic contribution (<8 mV).

Typically the redox contribution is responsible for strong negative self-potential anomalies [e.g., *Frischknecht et al.*, 1983; *Corwin*, 1989; *Naudet et al.*, 2003, 2004]. The redox mechanism by *Sato and Mooney* [1960] presents a plausible source for self-potential anomalies around vertical metallic conductors located into the ground.

[20] As *Naudet et al.* [2003], we look for separating the two self-potential contributions. One may ask if it would be ever possible to observe the electrokinetic component. The response to this question was partly answered by *Revil et al.* [2002], who observed that during a self-potential monitoring experiment, the signal-to-noise ratio of the potential change exceeded by two orders of magnitude the signal-to-noise ratio of the static self-potential map. Indeed, metallic (and other) noise sources are very common in areas where streaming potential surveys are conducted. Therefore it is always best, when possible, to conduct the self-potential surveys under at least two different flow conditions (e.g., full flow versus no flow for a well field, high water level versus low water level for a dam). So despite the modest amplitude of the electrokinetic contribution (<10 mV, see below), it is possible to observe this contribution quite well in the field as shown next.

[21] The monitoring network of electrodes was activated at 1017 LT. The pump was shutdown at 1038 LT and the electrical response was monitored during 3 hours (180′) as stated above. The experiment was stopped at 1333 LT when the water level was assumed to have reached formation B. By definition there is no electrokinetic contribution at the end of the experiment. Therefore, for each electrode, we can take a temporal reference at 1333 LT. In other words, this means that the electrical potential is set up to zero at that time (this would remove the redox component and reduce the static noise by assuming that these sources do not depend on time by comparison with the duration of the experiment). Of course, this step is not sufficient to remove entirely the noise.

[22] We observed a lot of spikes in the temporal series. These spikes were probably due to telluric currents and induction effects in the cables. To remove the spikes in the temporal series, we used a Fourier transform and a low-pass filter but by keeping the whole amplitude of the low-frequency self-potential variations. All these operations can be summarized by the flowchart of Figure 6. In Figures 7 and 8, we show the variations of the filtered electrical potentials recorded at some electrodes close to some piezometers for which the variations of the depth of the water table were measured. Note the concomitant variations of both the electrical potential and piezometric level as a function of time. This indicates unambiguously that part of the recorded electrical signal is associated with relaxation of the phreatic surface.

[23] We have also determined the difference of the electrical potential before the pump shutdown and that measured three hours after the pump shutdown for each electrodes. In Figure 9, we have plotted these differences as a function of the piezometric head difference. We observe that except for piezometer P9, all the data exhibit a linear trend with an apparent coupling coefficient equal to $-0.8$ mV m$^{-1}$.

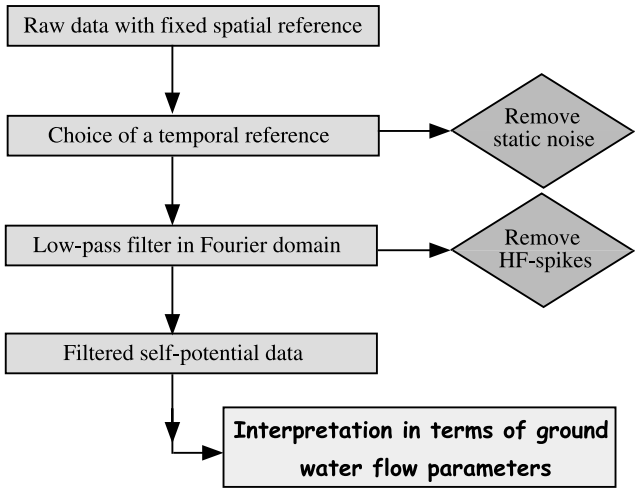


**Figure 6.** Flowchart used for the interpretation of the self-potential data in terms of groundwater flow parameters. To remove the high-frequency (HF) variations observed in the temporal sequences and attributed to telluric currents (or induction currents in the cables), we used a fast Fourier transform (FFT) and a low-pass filter. Then, by applying an inverse Fourier transform, we come back to the temporal domain.

### 3.3. Determination of the Equivalent Transmissivity

[24] To determine the equivalent homogeneous transmissivity and storage, we can apply the Theis solution to fit all the drawdown data sets obtained from the pumping test experiments. In this paper, we used a nonlinear least squares method [e.g., *Tarantola and Valette*, 1982] to invert the parameters of the Theis equation. This method is based on the minimization of the following cost function $\chi^2(\mathbf{a})$:

$$\mathrm{Min}\chi^2 \equiv \sum_{i=1}^{n}\sum_{j=1}^{t_{\max}}\left(\frac{h_{ij}-\hat{h}_{ij}}{\sigma_{ij}}\right)^2, \tag{26}$$

$$h_{ij} \equiv h_i^0 - w_{ij}, \tag{27}$$

$$\hat{h}_{ij} \equiv h_i^0 - \hat{w}_{ij}, \tag{28}$$

where the index $i \in \{1, \ldots, n\}$ represents the observation well numbers ($n = 5$ here), the index $j$ denotes the time index of the drawdown data $j \in \{1, \ldots, t_{\max}\}$, $h_{ij}$ are the observed hydraulic heads during the pumping test in the observation well $i$ at time $j$, $\hat{h}_{ij}$ are the hydraulic heads determined by means of Theis solution, $w_{ij}$ and $\hat{w}_{ij}$ are the associated drawdowns, and $\sigma_{ij}$ are the measurements errors (standard deviation) of the $i$th data point at time $j$, presumed to be known. To calculate $\hat{w}_{ij}$, we use the Theis equation [e.g., *Verruijt*, 1970]:

$$\hat{w}_{ij} = \frac{Q}{4\pi T} W\left(\frac{r_i^2 S}{4Tt_j}\right) \tag{29}$$

$$\hat{w}_{ij}\frac{Q}{4\pi T}\left[-0.5772 - \ln\left(\frac{r_i^2 S}{4Tt_j}\right) + \left(\frac{r_i^2 S}{4Tt_j}\right) - \frac{1}{2.2!}\left(\frac{r_i^2 S}{4Tt_j}\right) + \ldots\right], \tag{30}$$

where $W(u)$ is the Hantush well function. It follows from equations (26) and (30) that the cost function depends on $r$, $t$, $T$ and $S$. Sufficiently close to the minimum, we expect that the cost function $\chi^2(\mathbf{a})$ can be approximated by the quadratic form

$$\chi^2(\mathbf{a}) = \chi^2(\mathbf{a}_i) + (\mathbf{a}-\mathbf{a}_i)\cdot\nabla\chi^2(\mathbf{a}_i) + \frac{1}{2}(\mathbf{a}-\mathbf{a}_i)\cdot\nabla^2\chi^2(\mathbf{a}_i)\cdot(\mathbf{a}-\mathbf{a}_i). \tag{31}$$

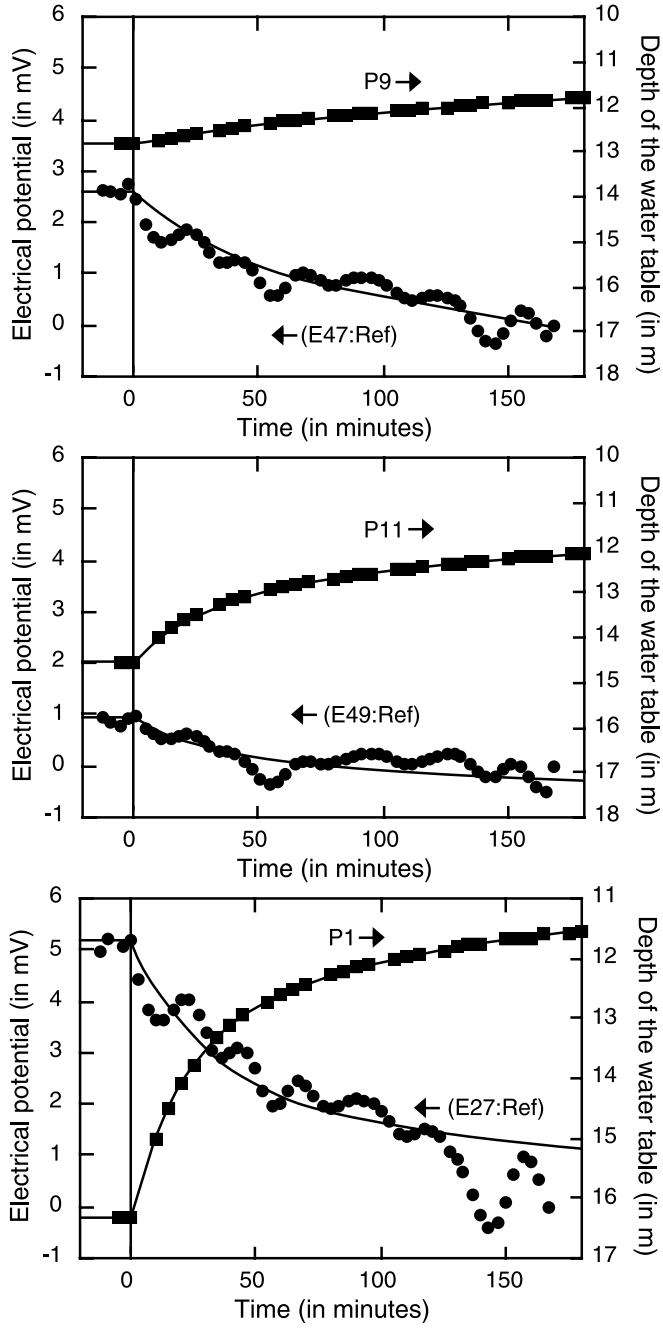


**Figure 7.** Variation of the self-potential with time for a selection of electrodes at different distances from the pumping well. Only a fraction of the data is shown. The time $t = 0$ indicates the shutdown of the pumping well. The "eye-guiding" curves are second-order polynomial fits of the data after the shutdown of the pump. The position of the reference electrode (Ref) is shown in Figure 3.

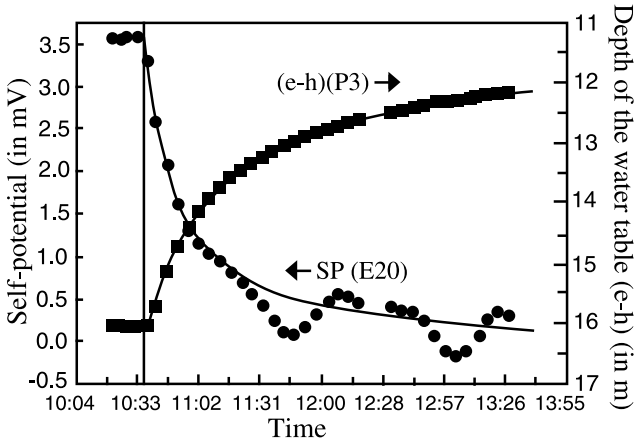


**Figure 8.** Comparison between the evolution of the depth of the water table ($e-h$) at piezometer P3 and the self-potential recorded at electrode E20. For the electrical potential, the final recorded values at the end of the experiment are used to define a temporal reference used to determine the electrical potential distribution during steady state pumping conditions. At $t$ = 1038 LT, the pump was shutdown. This time corresponds to the end of the steady state conditions and beginning of the relaxation of the phreatic surface toward its equilibrium state. The reference is shown at Figure 3.

[25] To find the minimum of the cost function, we can differentiate the function with respect to **a** and set the result equal to zero. This yields

$$\nabla\chi^2(\mathbf{a}) \cong \nabla\chi^2(\mathbf{a}_i) + (\mathbf{a}-\mathbf{a}_i)\cdot\nabla^2\chi^2(\mathbf{a}_i) = 0 \tag{32}$$

$$\nabla\chi^2(\mathbf{a}_i) + (\mathbf{a}-\mathbf{a}_i)\cdot[\mathbf{H}] = 0, \tag{33}$$

where [**H**] is the Hessian matrix of the cost function at $\mathbf{a}_i$. The step, $(\mathbf{a}-\mathbf{a}_i)$, to the next iteration point will be the solution of

$$(\mathbf{a}-\mathbf{a}_i)\cdot[\mathbf{H}] = -\nabla\chi^2(\mathbf{a}_i). \tag{34}$$

We want to determine the values of the transmissivity $T$ and the storage $S$ that minimizes the cost function, so we have

$$\frac{\partial\chi^2}{\partial T} = -2\sum_{i=1}^{n}\sum_{j=1}^{t_{\max}}\left[\frac{\left(h_{ij}-\hat{h}_{ij}\right)}{\sigma_{ij}}\right]\frac{\partial\hat{h}_{ij}}{\partial T} \tag{35}$$

$$\frac{\partial\chi^2}{\partial S} = -2\sum_{i=1}^{n}\sum_{j=1}^{t_{\max}}\left[\frac{\left(h_{ij}-\hat{h}_{ij}\right)}{\sigma_{ij}}\right]\frac{\partial\hat{h}_{ij}}{\partial S}. \tag{36}$$

Taking an additional partial derivative gives

$$\frac{\partial^2\chi^2}{\partial T_k\partial T_l} = -2\sum_{i=1}^{n}\sum_{j=1}^{t_{\max}}\frac{1}{\sigma_{ij}^2}\left[\frac{\partial\hat{h}_{ij}(\mathbf{a}_i)}{\partial T_k}\frac{\partial\hat{h}_{ij}(\mathbf{a}_i)}{\partial T_l}\right] - \left[h_{ij}-\hat{h}_{ij}(\mathbf{a}_i)\right]\frac{\partial^2\hat{h}_{ij}(\mathbf{a}_i)}{\partial T_k\partial T_l}, \tag{37}$$

$$\frac{\partial^2\chi^2}{\partial S_k\partial S_l} = -2\sum_{i=1}^{n}\sum_{j=1}^{t_{\max}}\frac{1}{\sigma_{ij}^2}\left[\frac{\partial\hat{h}_{ij}(\mathbf{a}_i)}{\partial S_k}\frac{\partial\hat{h}_{ij}(\mathbf{a}_i)}{\partial S_l}\right] - \left[h_{ij}-\hat{h}_{ij}(\mathbf{a}_i)\right]\frac{\partial^2\hat{h}_{ij}(\mathbf{a}_i)}{\partial S_k\partial S_l}. \tag{38}$$

If we start with a guessed value of $T$ and $S$ and we define

$$\mathbf{H}_{kl}^{T} \equiv \frac{\partial^2\chi^2}{\partial T_k\partial T_l}, \tag{39}$$

$$\mathbf{H}_{kl}^{S} \equiv \frac{\partial^2\chi^2}{\partial S_k\partial S_l}, \tag{40}$$

$$\mathbf{D}_{l}^{T} \equiv \frac{\partial\chi^2}{\partial T_l}, \tag{41}$$

$$\mathbf{D}_{l}^{S} \equiv \frac{\partial\chi^2}{\partial S_l}, \tag{42}$$

the improvement of the next step, $\Delta T$ and $\Delta S$, is given by the solution of the following equations:

$$\sum_{i=1}^{n}\sum_{j=1}^{t_{\max}}\mathbf{H}_{ij}^{T}\Delta T = \mathbf{D}_{i}^{T} \tag{43}$$

$$\sum_{i=1}^{n}\sum_{j=1}^{t_{\max}}\mathbf{H}_{ij}^{S}\Delta S = \mathbf{D}_{i}^{S}. \tag{44}$$

Then, the increments $\Delta T$ and $\Delta S$ can be added to the guess (a priori) values of $T$ and $S$ and used to reevaluate the

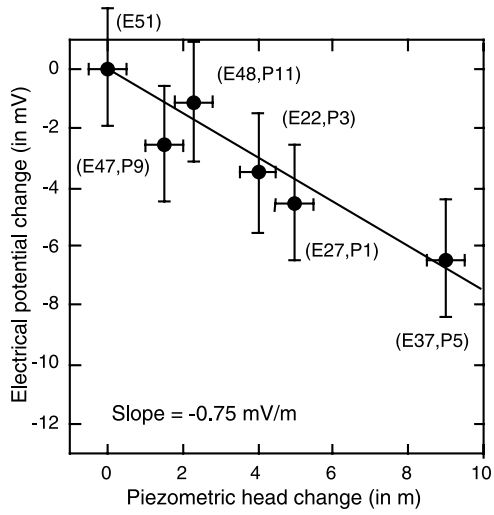


**Figure 9.** Self-potential change versus piezometric change during the relaxation of the phreatic surface. We use the electrodes close to each piezometer including the pumping well.

**Table 1.** Transmissivity and Storage Coefficient by Means of the Nonlinear Least Squares Method

| Pumping Well 5 | Observation Wells | | | | | Equivalent Parameters |
|---|---|---|---|---|---|---|
| | Well 1 | Well 3 | Well 7 | well 9 | Well 11 | |
| $T$ ($10^{-4}$), m$^2$ s$^{-1}$ | 1.04 | 1.05 | 1.13 | 1.52 | 1.30 | 1.22 |
| $S$ ($10^{-3}$) | 7.3 | 6.8 | 3.2 | 11.7 | 2.5 | 4.9 |

simulated head $\hat{h}$. If the cost function given by equation (26) does not meet a given criterion of convergence, the procedure is repeated until a fixed number of iteration or until the criterion is finally reached. Applying this numerical procedure to the present pumping test, we obtain the transmissivities and storativities reported in Table 1.

### 3.4. Uncertainty Analysis

[26] The inverse method proposed in the previous section was implemented to utilize all information available in a pumping test with several observation wells. In fact, our method minimizes the square mean error between the measured drawdowns in all observation wells and the theoretical drawdowns obtained by means of the Theis solution (equation (30)). It is well noted that Theis solution implies the hypothesis of homogenous and isotropic porous media. On the other hand, in a natural aquifer its characteristic properties vary over a few orders of magnitude. Extensive tabulations of data for many different types of aquifers and soils clearly establish that such variations in hydraulic properties are the rule than the exception [e.g., *Gelhar*, 1993]. In such as approach the transmissivity obtained with the Theis solution has to be considered as an effective transmissivity. Gelhar showed that for a two-dimensional flow, with no trend in mean log conductivity and a statistically isotropic ln($K$) field, the effective conductivity is simply the geometric mean [*Gelhar*, 1993]

$$K_{ij} = K_g \delta_{ij}, \tag{45}$$

with $i, j = 1, 2$. Otherwise, if we apply the geometric mean on the single transmissivities evaluated for each observation wells, we obtain $T_g = 1.20 \times 10^{-4}$ m$^2$ s$^{-1}$, which is very close to the equivalent transmissivity obtained with our inverse approach ($T_{eff} = 1.22 \times 10^{-4}$ m$^2$ s$^{-1}$). Such as result

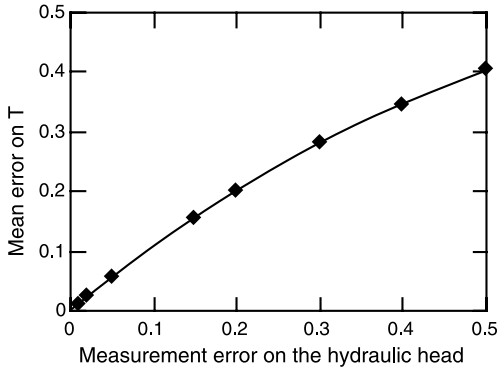


**Figure 10.** Mean errors on the hydraulic transmissivity versus the measurement errors as a percentage of hydraulic head observed.

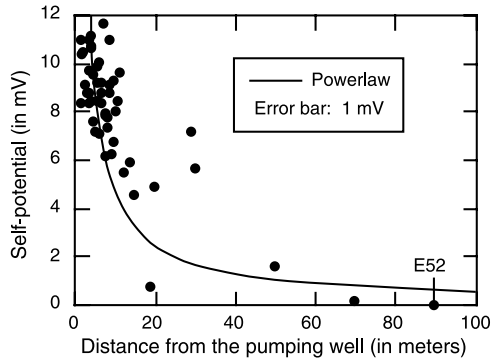


**Figure 11.** Variation of the electrical potential with the distance to the pumping well. The electrode E52 is chosen as a reference. In steady state conditions, the electrical potential decreases as the inverse of the distance from the pumping well.

is a confirmation of the validity of the strategy applied to determine effective transmissivity using head observations of all observation wells.

[27] Another source of error could be measurement errors in drawdowns. To investigate the impact of these errors, we generated random drawdowns measurement errors with a mean equals to 2 cm (i.e., the accuracy of the divers used in the pumping test) and a variance that is equal to a specified fraction of the head variance for each observation well. Drawdowns at the monitoring locations were then perturbed with these errors and then were used in the inversion algorithm. Several numerical experiments were conducted to examine the impact of hypothetical measurement errors of the drawdowns on the equivalent transmissivity. Results of the inversion show that the estimate by our inverse method is not sensitive to these errors.

[28] Successively we have perturbed the drawdowns measurement errors as before but with a trend. This trend was evaluated as a percentage of the hydraulic head. Monte Carlo simulations, using 200 random perturbed drawdowns, with a fixed mean and variance and variable trends, were conducted to estimate the errors in the hydraulic transmissivity. In this second case, results show that the estimates are more sensitive to the errors. The effects of trend measurement errors on the hydraulic transmissivity estimates are shown in Figure 10, as we can see, the norm of error grows with the error increases. However, transmissivity error becomes significant only for measurement errors greater than the maximum error admitted for the divers used in the experimental pumping test.

### 3.5. Interpretation of the Self-Potential Data

[29] We first interpret the data in steady state conditions. We have plotted the electrical potential data as a function of the distance to the pumping well in Figure 11. To draw Figure 11, all the electrical potential data have been referenced at 1333 LT (temporal reference). The application of a power law relationship to these data yields $\varphi(r) \approx 39.63 r^{-0.93}$, where the electrical potential is expressed here in mV, $r$ is in meters, and the correlation coefficient is quite low ($R = 0.54$). This relationship can be compared to the relationship developed in section 2, equation (21), which gives $\varphi(r) \approx A/r$, where $A = -C'Q^2/4\pi^2K^2H_0^2$ (such depen-

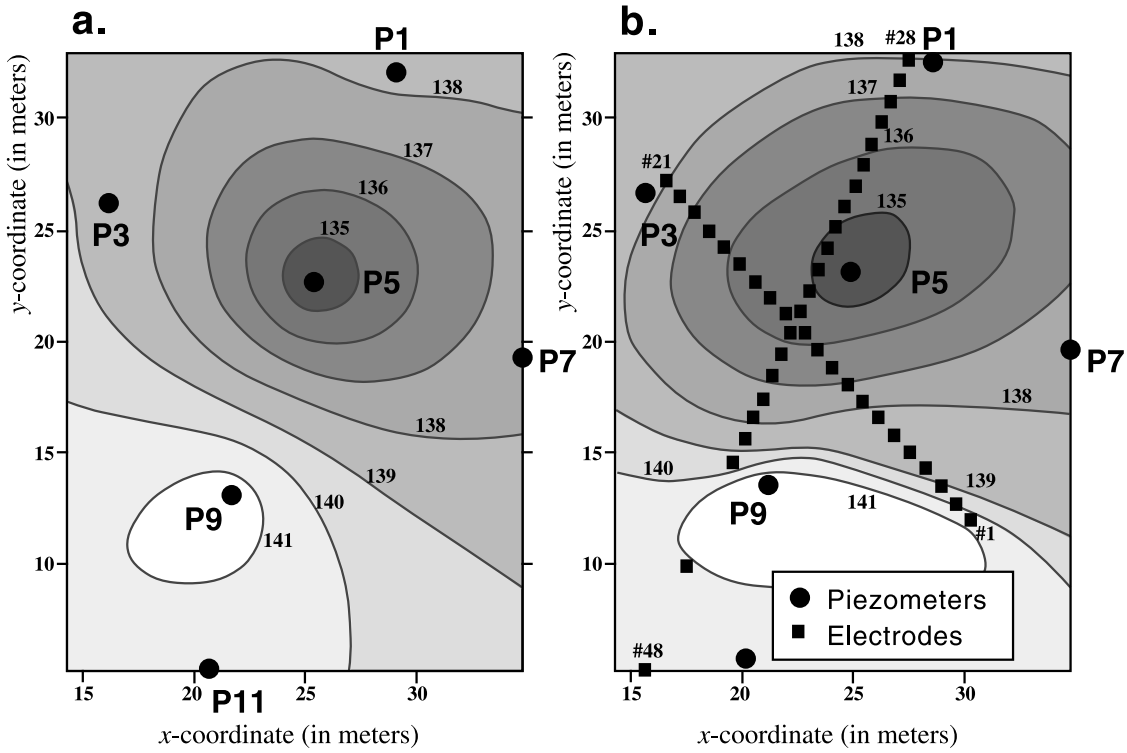


**Figure 12.** Determination of the piezometric surface in steady state conditions. Comparison between (b) the piezometric surface determined using the piezometric data plus the self-potential data and (a) the piezometric surface determined with only the piezometric data. Note the marked heterogeneity in the vicinity of well P9 (coupling coefficient used −0.8 mV/m, reference electrode E53, time reference 1332 LT).

dence was also observed by P. Gex (personal communication, 2003)). To interpret the data of Figure 11 with this equation, the first point is to determine the value of the electrokinetic coupling coefficient.

[30] The electrokinetic coupling coefficient $C'$ depends mainly on the value of the electrical conductivity of the groundwater according to an empirical relationship developed by *Revil et al.* [2003a] (for an aquifer, the coupling coefficient is relatively independent of the texture of the porous material). We measured the conductivity of the groundwater in the field and we found a value of 0.0915 S $m^{-1}$ at 25°C. Note that this yields a value for the electrical formation factor in the range 5–20 for sands and gravels using the resistivity tomography shown in Figure 2. These range of values are in agreement with the formation factor estimated in a similar aquifer by *Naudet et al.* [2004].

[31] Using the relationship developed by *Revil et al.* [2003a] between the electrokinetic coupling term and the electrical conductivity of the pore water, we obtain $C' = -1.6$ mV $m^{-1}$. However, if the pore water contains a high proportion of divalent cations like $Ca^{2+}$, the zeta potential entering the determination of the electrokinetic coupling coefficient is twice as small as that for monovalent cations at the same electrical conductivity of the pore water solution [*Lorne et al.*, 1999]. Therefore we take $C' \approx -0.8$ mV $m^{-1}$ as a representative value for the electrokinetic coupling coefficient in the main aquifer. This value should be considered only as a rough estimate. We note however that this value compares favorably with the apparent coupling coefficient determined from the data plotted Figure 9.

[32] Taking $A = 39.63$ mV m (determined above), $C' = -0.8$ mV $m^{-1}$, $H_0 = 20$ m (measured, Figure 2), $Q = 2.7 \times 10^{-3}$ $m^3$ $s^{-1}$, and $K = (-C'Q^2/4\pi^2 H_0^2 A)^{1/2}$ yields a hydraulic conductivity equal to $2.2 \times 10^{-6}$ m $s^{-1}$. The uncertainty associated with this estimate depends directly on the uncertainty associated with the estimation of the coupling coefficient $C'$, which is difficult to evaluate. Using the fact that $T = Kb$, where $b$ is the initial saturated thickness of the aquifer ($b \approx 44$ m), the equivalent transmissivity of the main aquifer is around $1.0 \times 10^{-4}$ $m^2$ $s^{-1}$. This value is consistent with the equivalent transmissivity value determined in section 3.3 and Table 1 by means of the nonlinear least squares method. All the information available can be used to reconstruct the shape of the water table. This includes the direct measurements of the piezometric levels and the self-potential data converted in piezometric data using the relationship defined in Figure 9. The final result is shown Figure 12.

[33] We discuss now the relaxation of the electrical potential associated with the relaxation of the phreatic surface after the shutdown of the pump. For all piezometers except P9, the variation of the hydraulic head scales approximately with the logarithm of time (Figure 13). The electrical potentials are shown as a function of the logarithm of the ratio $t/t'$ in Figure 14 ($t'$ is the time since pumping stopped, $t = t' + \delta t$ is the time since pumping started, and $\delta t = 5854.7$ min is the duration of the pumping test). The data show a linear trend as predicted

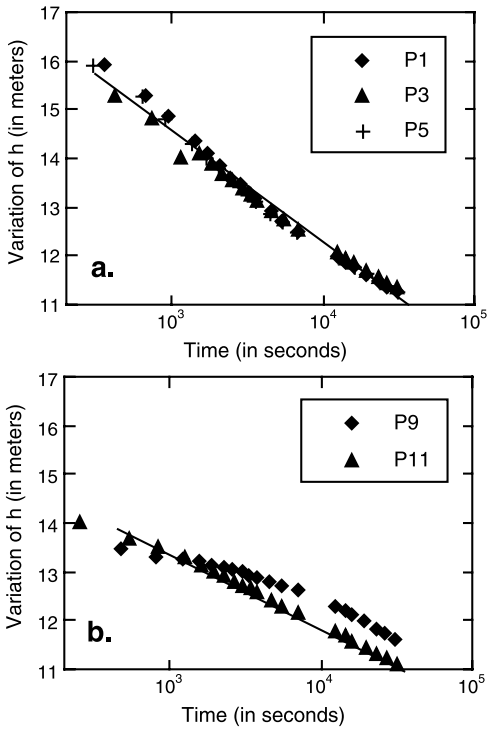


**Figure 13.** Variation of the hydraulic head versus time for the different piezometers. For all piezometers except P9, the variation of the hydraulic head scales approximately with the logarithm of time.

by the equation (25). Writing equation (25) as $\varphi = \varphi_0 + \alpha \log(t/t')$, we obtain $\alpha$ in the range 1.8–1.4 mV. Using the fact that according to equation (25), $\alpha = -C'2.3Q/4\pi T$. Taking this value and $C' = -0.8$ mV m$^{-1}$, $Q = 2.7 \times 10^{-3}$ m$^3$ s$^{-1}$, we obtain $T$ in the range $(2.2–2.8) \times 10^{-4}$ m$^2$ s$^{-1}$. These values are consistent with the results reported in Table 1.

## 4. Concluding Statements

[34] In this paper, we have shown that measurable electrical signals can be recorded at the ground surface during a pumping test experiment including the relaxation phase of the phreatic surface after the pump shutdown. The electrical signals can be understood by solving the coupled hydroelectric problem including the very high conductivity of the metallic casing. The interpretation scheme is still in its infancy as only ideal aquifers have been considered here. Extensions of this model would include (1) the determination of the hydraulic conductivity distribution around the pumping well by assuming that the hydraulic conductivity depends on both the azimuth and the distance to the pumping well and (2) the inclusion of the electrical resistivity distribution in the inverse problem. Indeed, the self-potential method cannot be used as a stand-alone technique. The recent development of multichannel resistivity meters implies that electrical resistivity tomography (ERT) can be combined with self-potential tomography (SPT) to go one step further in the determination of the geometry of the hydraulic response during a pumping test experiment. This opens exciting perspectives in the monitoring of groundwater flow in real time and the determination of the distribution of the hydraulic transmissivity using for example the successive linear estimator [*Yeh et al.*, 1996] or a maximum likelihood estimation procedure for that purpose. In addition, numerical modeling can be used to address the forward problem for an arbitrary physical property distribution (see, for example, *Sheffer and Howie* [2001, 2003], who used MODFLOW-3D as a "front end" to calculate the seepage flow and then calculate the resulting self-potential field).

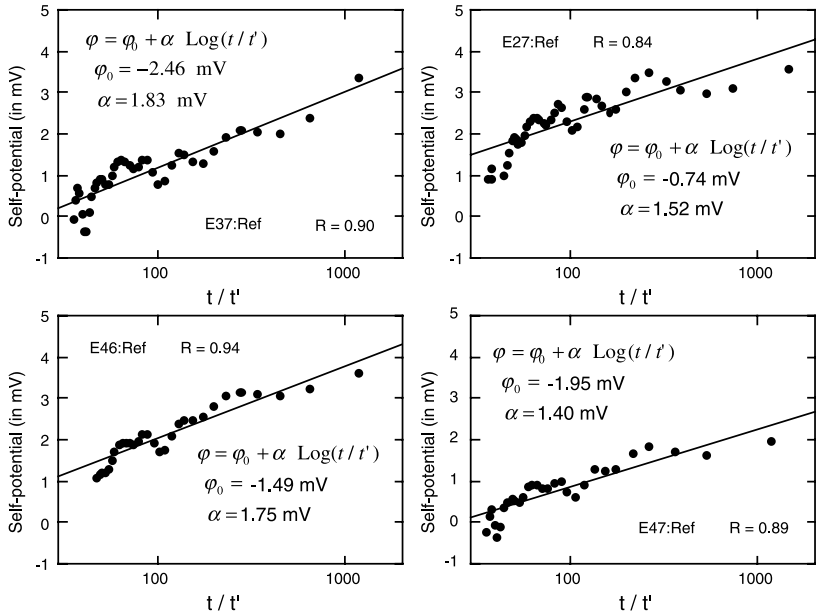


**Figure 14.** Variation of the electrical potential versus the ratio $t/t'$ during the relaxation of the phreatic surface following the shutdown of the pumping well. The position of the reference electrode (Ref) is shown Figure 3.

[35] **Acknowledgments.** One of us, André Revil, thanks Bruno Hamelin for his support at CEREGE. We thank ACI "Eau et Environnement" (Bernard Dupré) and PNRH (through a project with Claude Doussan, INRA, Avignon, France) for financial supports. A.R. thanks Pierre Gex and Maurice Aubert for stimulating and fruitful discussions about self-potential signals. We thank Robert Corwin, David Fitterman, and Phil Wannamaker for their works and constructive comments regarding this paper.

## References

Aubert, M., and Q. Yéné Atangana (1996), Self-potential method in hydrogeological exploration of volcanic areas, *Ground Water*, *34*, 1010–1016.

Bernabé, Y. (1998), Streaming potential in heterogeneous networks, *J. Geophys. Res.*, *103*, 20,827–20,841.

Birch, F. S. (1993), Testing Fournier's method for finding water table from self-potential, *Ground Water*, *31*, 50–56.

Birch, F. S. (1998), Imaging the water table by filtering self-potential profiles, *Ground Water*, *36*, 779–782.

Bogoslovsky, V. A., and A. A. Ogilvy (1973), Deformations of natural electric fields near drainage structures, *Geophys. Prospect.*, *21*, 716–723.

Cassiani, G., and G. Christakos (1998), Analysis and estimation processes with nonhomogeneous spatial variation using secondary information, *Math. Geol.*, *30*(1), 57–76.

Cassiani, G., and M. A. Medina (1997), Incorporating auxiliary geophysical data into ground-water flow parameter estimation, *Ground Water*, *35*, 79–91.

Cassiani, G., G. Böhm, A. Vesnaver, and R. Nicolich (1998), A geostatistical framework for incorporating seismic tomography auxiliary data into hydraulic conductivity estimation, *J. Hydrol.*, *206*, 58–74.

Corwin, R. F. (1989), Data quality for engineering self-potential surveys, in *Proceedings, International Symposium on the detection of subsurface flow phenomena, Lecture Notes in Earth Sciences*, Springler-Verlag, Berlin, pp. 51–72.

Corwin, R. F., and H. F. Morrison (1977), Self-potential variations preceding earthquakes in Central California, *Geophys. Res. Lett.*, *4*(4), 171–174.

Darnet, M., G. Marquis, and P. Sailhac (2003), Estimating aquifer hydraulic properties from the inversion of surface Streaming Potential (SP) anomalies, *Geophys. Res. Lett.*, *30*(13), 1679, doi:10.1029/2003GL017631.

Domenico, P. A., and F. W. Schwartz (1997), *Physical and Chemical Hydrogeology*, 2nd ed., John Wiley, Hoboken, N. J.

Fitterman, D. V. (1978), Electrokinetic and magnetic anomalies associated with dilatant regions in a layered Earth, *J. Geophys. Res.*, *83*, 5923–5928.

Fitterman, D. V. (1979), Theory of electrokinetic-magnetic anomalies in a faulted half-space, *J. Geophys. Res.*, *84*, 6031–6040.

Fournier, C. (1989), Spontaneous potentials and resistivity surveys applied to hydrogeology in a volcanic area: Case history of the Chaîne des Puys (Puy-de-Dôme, France), *Geophys. Prospect.*, *37*, 647–668.

Friborg, J. (1996), Experimental and theoretical investigations into the streaming potential phenomenon with special reference to applications in glaciated terrain, Ph.D. Thesis, Div. of Appl. Geophys., Lulea Univ. of Technol., Lulea, Sweden.

Frischknecht, F. C., L. Muth, R. Grette, T. Buckley, and B. Kornegay (1983), Geophysical methods for locating abandoned wells, *U.S. Geol. Surv. Open File*, *83-702*.

Fujinawa, Y., T. Matsumoto, and K. Takahashi (2002), Modeling confined pressure changes inducing anomalous electromagnetic fields related to earthquakes, *J. Appl. Geophys.*, *49*, 101–110.

Furness, P. (1992), Modeling spontaneous polarization potentials with a new integral equation, *J. Appl. Geophys.*, *29*, 143–155.

Gelhar, L. W. (1993), *Stochastic Subsurface Hydrology*, Prentice-Hall, Old Tappan, N. J.

Lorne, B., F. Perrier, and J. P. Avouac (1999), Streaming potential measurements: 1. Properties of the electrical double layer from crushed rock samples, *J. Geophys. Res.*, *104*, 17,857–17,877.

Naudet, V., A. Revil, J.-Y. Bottero, and P. Bégassat (2003), Relationship between self-potential (SP) signals and redox conditions in contaminated groundwater, *Geophys. Res. Lett.*, *30*(21), 2091, doi:10.1029/2003GL018096.

Naudet, V., A. Revil, E. Rizzo, J.-Y. Bottero, and P. Bégassat (2004), Groundwater redox conditions and conductivity in a contaminant plume from geoelectrical investigations, *Hydrol. Earth Syst. Sci.*, *8*(1), 8–22.

Perrier, F., et al. (1997), A one year systematic study of electrodes for long period measurements of the electric field in geophysical environments, *J. Geomagn. Geoelectr.*, *49*, 1677–1696.

Perrier, F., M. Trique, B. Lorne, J. P. Avouac, S. Hautot, and P. Tarits (1998), Electrical variations associated with yearly lake level variations, *Geophys. Res., Lett.*, *25*, 1955–1958.

Perrier, F., G. R. Chitrakar, T. Froidefond, D. Tiwari, U. Gautam, B. Kafle, and M. Trique (2002), Estimating streaming potentials associated with geothermal circulation at the main central trust: An example from Tatopani-Kodari hot spring in central Nepal, *J. Nepal Geol. Soc.*, *26*, 17–27.

Petiau, G. (2000), Second generation of lead-lead chloride electrodes for geophysical applications, *Pure Appl. Geophys.*, *157*, 357–382.

Poldini, E. (1938), Geophysical exploration by spontaneous polarization methods, *Mineral. Mag.*, *59*, 278–282, 347–352.

Rabaute, A., A. Revil, and E. Brosse (2003), In situ mineralogy and permeability logs from downhole measurements: Application to a case study in clay-coated sandstone formations, *J. Geophys. Res.*, *108*(B9), 2414, doi:10.1029/2002JB002178.

Revil, A., and P. Leroy (2004), Governing equations for ionic transport in porous shales, *J. Geophys. Res.*, *109*, B03208, doi:10.1029/2003JB002755.

Revil, A., L. M. Cathles, S. Losh, and J. A. Nunn (1998), Electrical conductivity in shaly sands with geophysical applications, *J. Geophys. Res.*, *103*, 23,925–23,936.

Revil, A., D. Hermitte, M. Voltz, R. Moussa, J.-G. Lacas, G. Bourrié, and F. Trolard (2002), Self-potential signals associated with variations of the hydraulic head during an infiltration experiment, *Geophys. Res. Lett.*, *29*(7), 1106, doi:10.1029/2001GL014294.

Revil, A., V. Naudet, J. Nouzaret, and M. Pessel (2003a), Principles of electrography applied to self-potential electrokinetic sources and hydrogeological applications, *Water Resour. Res.*, *39*(5), 1114, doi:10.1029/2001WR000916.

Revil, A., G. Saracco, and P. Labazuy (2003b), The volcano-electric effect, *J. Geophys. Res.*, *108*(B5), 2251, doi:10.1029/2002JB001835.

Revil, A., A. Finizola, F. Sortino, and M. Ripepe (2004), Geophysical investigations at Stromboli volcano, Italy: Implications for ground water flow, *Geophys. J. Int.*, *157*(1), 426–440.

Sato, M., and H. M. Mooney (1960), The electrochemical mechanism of sulfide self-potentials, *Geophysics*, *25*(1), 226–249.

Semenov, A. S. (1980), *Electrical Prospecting With the Natural Electric Field Method* (in Russian), 3rd ed., 448 pp., Nedra, St. Petersburg, Russia.

Sheffer, M. R. (2002), Response of the self-potential method to changing seepage conditions in embankment dams, M.A.Sc. thesis, Dep. of Civ. Eng., Univ. of B. C., Vancouver, April 2002.

Sheffer, M. R., and J. A. Howie (2001), Imaging subsurface seepage conditions through the modelling of streaming potential, in *Proceedings of 54th Canadian Geotechnical Conference*, pp. 1094–1101, Can. Geotech. Soc., Calgary, Alberta.

Sheffer, M. R., and J. A. Howie (2003), A numerical modelling procedure for the study of the streaming potential phenomenon in embankment dams, paper presented at Symposium on the Application of Geophysics to Engineering and Environmental Problems, Environ. and Eng. Geophys. Soc., San Antonio, Tex.

Sill, W. R. (1983), Self-potential modeling from primary flows, *Geophysics*, *48*, 76–86.

Sobolev, S. L. (1989), *Partial Differential Equations of Mathematical Physics*, 427 pp., Dover, Mineola, N. Y.

Tarantola, A., and B. Valette (1982), Generalized nonlinear inverse problems solved using the least squares criterion, *Rev. Geophys.*, *20*, 219–232.

Titov, K., V. Loukhmanov, and A. Potapov (2000), Monitoring of water seepage from a reservoir using resistivity and self-polarization methods: Case history of the Petergoph fountain water supply system, *First Break*, *18*, 431–435.

Titov, K., Y. Ilyin, P. Konosavski, and A. Levitski (2002), Electrokinetic spontaneous polarization in porous media: Petrophysics and numerical modeling, *J. Hydrol.*, *267*, 207–216.

Troisi, S., C. Fallico, S. Straface, and E. Migliari (2000), Application of kriging with external drift to estimate hydraulic conductivity from electrical-resistivity data in unconsolidated deposits near Montalto Uffugo, Italy, *Hydrogeol. J.*, *8*, 356–367.

Verruijt, A. (1970), *Theory of Groundwater Flow*, Gordon and Breach, Newark, N. J.

Wilt, M. J., and D. K. Butler (1990), Numerical modeling of SP anomalies: Documentation of program SPPC and applications: Geotechnical applications of the self-potential (SP-) method, *Rep. 4, Tech. Rep. REMR-GT-6*, Waterways Exper. Stn., U.S. Army Corps of Eng., Vicksburg, Miss.

Yeh, T.-C. J., M. Jin, and S. Hanna (1996), An iterative stochastic inverse method: Conditional effective transmissivity and hydraulic head fields, *Water Resour. Res.*, *32*, 85–92.

A. Revil and B. Suski, Département d'Hydrogéophysique et Milieux Poreux, CNRS, CEREGE, F-1345 Aix-en-Provence cedex 04, France. (revil@cerege.fr)

E. Rizzo, Institute of Methodologies for Environmental Analysis, IMAA-CNR, I-85050 Tito Scalo, Potenza, Italy.

S. Straface and S. Troisi, Soil Conservation Department, University of Calabria, I-87040 Cosenza, Italy.